**PCCP**

# Aromaticity of Unsaturated BEC4 Heterocycles (E = N, P, As, Sb, O, S, Se, Te)

SCHOLARONE™
Manuscripts

# Journal Name

# Aromaticity of Unsaturated BEC$_4$ Heterocycles (E = N, P, As, Sb, O, S, Se, Te)$^\dagger$

Paul A. Brown$^\ddagger$, Caleb D. Martin, and Kevin L. Shuford$^*$

A compendium of pnictogen and chalcogen substituted boron heterocycles were assessed for their aromatic character by first principles density functional theory. Group-15 and Group-16 elements were placed at the ortho-, meta-, and para-positions of six-membered rings relative to boron to assess their impact on the aromaticity of the unsaturated heterocycles. Aromaticity was analyzed by a multidimensional approach using nuclear independent chemical shifts, gauge-including magnetically induced current, as well as natural bond orbital and natural resonance theory analyses. Based on these methods, we observe a general decline of aromaticity in heavier pnictaborines while the chalcogen analogues maintain relatively strong aromatic character. These general trends result from complementary $\pi$-$\pi^*$ natural bond order interactions that sustain resonance within the ring of each heterocycle establishing a pattern of cyclic delocalization. Consequently, natural resonance theory displays strong resonance, which is corroborated with the signed modulus of ring current, toroidal vortices of current maps, and elevated average induced current throughout the ring. The 1,3-configurations for pnictaborines and chalcogenaborines are generally more aromatic compared to the 1,2- and 1,4-isomers, which contain $\pi$-holes that limit diatropism within the heterocycles. However, an energetic trend favors the 1,2-heterocycles in both groups, with a few exceptions driven in large-part by $\pi$-donation of the lone pair on the heteroatom to the $p_z$ orbital on the adjacent boron resulting in stabilization. The importance of planarity for high aromaticity is demonstrated, especially in the pnictaborine isomers where pyramidalization at the pnictogen is favored, while bond regularity seems a less important criterion.

## 1 Introduction

Group 13-15 and Group 13-16 combinations have become an integral isoelectronic or isostructural complement to aromatics like benzene. Such compounds, particularly the BN-unit or BO-unit, have had a range of applications since their synthesis beginning with Dewar and White in the 1950-60s[1–5]. Such organic/inorganic compounds have found uses in biomedical applications, materials science, frustrated Lewis acid-base pair chemistry, organometallic $\pi$-ligands, and polymerization catalysis, expanding chemical complexity and functional utility across many areas of science[6–15]. A fundamental molecular property governing the chemistry of such compounds is their aromaticity. Understanding aromaticity in this class of molecules is of crucial importance as it underscores the molecular complexion of such

compounds. In particular, molecular properties like optical response, chemical reactions (e.g., electrophilic aromatic substitutions), ring current, $\pi$-stacking, cation-$\pi$ interactions, and so on are all influenced by aromaticity[16,17].

Aromaticity is a salient molecular property emerging from a cyclic assembly of elements whose arrangement permits electron delocalization over the entire ring[16]. Notable criteria for aromaticity in molecules are bond equilibration, planarity, decreased reactivity, enhanced stability, and magnetic character[16]. Because of the influence of aromaticity on molecular characteristics, it is of great interest to quantify the aromatic signatures for a given conjugated cyclic molecule. Earlier attempts to quantify the aromaticity of 1,2-dihydro-1,2-azaborine were based, initially, on theory and were substantiated experimentally[18–22]; however, other isosteric combinations have not been widely studied. It is notable that criteria for aromaticity, such as ring current and delocalization, are not always directly related to stabilization[21]. Aromaticity has been regarded as a multidimensional property, necessitating the use of numerous methods for an appropriate analysis[23]. For instance, the harmonic oscillator model approximation and its variants use well-known unsaturated molecules as a ref-

Address: Department of Chemistry & Biochemistry, Baylor University, One Bear Place #97348, Waco, TX 76798-7348, United States. E-mail: kevin_shuford@baylor.edu
$\dagger$ Electronic Supplementary Information (ESI) available: Results for the entire dataset of both molecular classes as well as xyz coordinate files are available. See DOI: 00.0000/00000000.
$\ddagger$ Present address: U.S. Naval Research Laboratory, Chemistry Division, Code 6189, 4555 Overlook Avenue, SW Washington, DC 20375, United States.

erence to assess a cyclic compound possessing similar chemical bonding[23]. However, such approaches could have many different reference compounds, and thus offer no intrinsic first principles basis for characterizing aromatic character. Consequently, it is important to select metrics that can evaluate aromatic signatures unique to a given molecule.

In this article, we explore the structure, thermodynamic stability, and aromatic character of both pnictogen (Group-15) and chalcogen (Group-16) elements substituted within unsaturated boron heterocycles (BEC$_4$, E=pnictogen or chalcogen). We apply density functional theory (DFT) to understand the periodic trends that emerge and how the aromaticity evolves within both groups. In this regard, we use nuclear independent chemical shifts (NICS) with the gauge-independent atomic orbital method.[16,24–29] The use of NICS is reasonable here as the ring sizes deviate little over both groups, and they are determined from the second variation of the Kohn-Sham ground state energy with respect to the magnetic field and local magnetic moment on each element. Since NICS values contain a local sample of the molecular shielding tensor, we include the signed modulus of the ring current to display, unequivocally, diamagnetic and paramagnetic contributions to the molecular current density within the gauge-including magnetically induced current (GIMIC) approach.[23,30–35] Using the GIMIC method, we show the induced current field 1 Å above the molecular plane can corroborate NICS values for the molecules reported here with the aid of current density maps and average induced current through each endocyclic bond. Finally, we apply natural bond orbital (NBO) and natural resonance theory (NRT) to understand bonding motifs and resonance structures across both groups that promote aromaticity through principle delocalizations among $\pi$-$\pi^*$ natural bond orbitals.

## 2 Theoretical Methods

The calculations on pnictaborines and chalcogenaborines used density functional theory[36,37]. Structural optimizations and electrostatic potential surfaces were performed within the Gaussian 09 suite.[38] From the optimized structures, the nuclear independent chemical shifts were computed, NICS$_{ISO}$(1) and NICS$_{ZZ}$(1), with the gauge-independent atomic orbital (GIAO) method[16,24,26]. The Heyd-Scuseria-Ernzerhof screened hybrid density functional approximation (HSE06) was employed with all Gaussian 09 computations[39–42]. We used a def2-QZVPPD basis set with tight convergence criteria to optimize heterocycles containing N−As and O−Se elements and effective-core potentials for antimony and tellurium.[43–45] Ring currents were computed using the GIMIC (Gauge-including magnetically induced current) code interfaced with Gaussian 09.[30–35] From GIMIC, current maps, signed moduli of the current density, and average induced current through each bond along the ring were computed to assess molecular contributions to the overall aromaticity.[30–35] The optimized structures were ported into Orca 3.0.3 for single-point energy computations to interface with NBO 6.0, where natural bond orbital (NBO) and natural resonance theory (NRT) analysis were applied[46–51]. Since Orca does not employ HSE06, we utilized the pure exchange-correlation functional of Perdew-Burke-Ernzerhof (PBE0) for all single-point calculations

used for NBO and NRT analysis[52,53]. Orca single point calculations were completed with a def2-TZVPPD basis for N−As and O−Se, while a relativistic correction and effective core-potential (def2-TZVPP/J,def2-TZVPP) was applied to the heavier antimony and tellurium-substituted heterocycles.[45,54–56]

## 3 Results and Discussion

In this section, we will focus discussion on the properties of the pnictogen and chalcogen substituted boron heterocycles deemed most aromatic based upon our analysis. These quintessential cases within each group will be contrasted to their least aromatic counterparts to provide context on the range of aromaticity for these heterocycles. The full dataset describing all molecules investigated can be found in the Supplemental Information (SI) accompanying this article.

**Table 1** Nuclear independent chemical shifts (NICS) and average induced current density ($\mathscr{J}$) for all heterocycles. NICS values are computed 1 Å above the molecular plane and in units of $ppm$. $\mathscr{J}$ is reported as diatropic ($\mathscr{J}^{Dia}$), paratropic ($\mathscr{J}^{Para}$), and total current density ($\mathscr{J}^{Total}$) in units of $nAT^{-1}$. As a reference, the values for benzene are the following: NICS$_{ZZ}$(1) = -30.44 $ppm$, NICS$_{ISO}$(1) = -10.14 $ppm$, $\mathscr{J}^{Dia}$ = 17.09 $nAT^{-1}$, $\mathscr{J}^{Para} = -4.98$ $nAT^{-1}$, and $\mathscr{J}^{Total} = 12.06$ $nAT^{-1}$. We employ the shorthand $o$-BN, for example, to refer to 1,2-dihydro-1,2-azaborine (i.e. a heterocycle with nitrogen substituted ortho to boron).

| Molecule | NICS$_{ZZ}$(1) | NICS$_{ISO}$(1) | $\mathscr{J}^{Dia}$ | $\mathscr{J}^{Para}$ | $\mathscr{J}^{Total}$ |
|---|---|---|---|---|---|
| $o$-BN | -21.50 | -7.10 | 14.14 | -5.28 | 8.86 |
| $m$-BN | -26.60 | -8.97 | 15.52 | -4.80 | 10.72 |
| $p$-BN | -20.87 | -7.28 | 14.03 | -5.39 | 8.64 |
| $o$-BP | -23.82 | -8.82 | 15.17 | -4.61 | 10.56 |
| $m$-BP | -23.31 | -8.18 | 14.51 | -4.32 | 10.19 |
| $p$-BP | -9.62 | -3.89 | 11.35 | -6.07 | 5.27 |
| $o$-BAs | -12.29 | -4.92 | 13.09 | -5.97 | 7.12 |
| $m$-BAs | -18.51 | -8.17 | 14.91 | -4.91 | 10.00 |
| $p$-BAs | -3.67 | -2.50 | 10.32 | -6.60 | 3.72 |
| $o$-BSb | -2.12 | -1.75 | 10.42 | -7.18 | 3.24 |
| $m$-BSb | -8.42 | -3.93 | 12.34 | -5.60 | 6.74 |
| $p$-BSb | -4.38 | -1.75 | 9.23 | -6.96 | 2.27 |
| $o$-BO | -16.53 | -5.88 | 12.35 | -5.25 | 7.10 |
| $m$-BO | -23.85 | -8.66 | 14.79 | -4.83 | 9.95 |
| $p$-BO | -16.53 | -5.87 | 12.71 | -5.70 | 7.01 |
| $o$-BS | -19.66 | -7.09 | 14.83 | -5.72 | 9.11 |
| $m$-BS | -25.36 | -8.60 | 15.90 | -4.90 | 11.00 |
| $p$-BS | -19.76 | -7.15 | 13.75 | -5.53 | 8.22 |
| $o$-BSe | -18.85 | -7.07 | 14.39 | -5.55 | 8.84 |
| $m$-BSe | -25.04 | -8.79 | 15.99 | -4.93 | 11.06 |
| $p$-BSe | -15.25 | -5.91 | 13.26 | -5.71 | 7.55 |
| $o$-BTe | -17.12 | -7.66 | 14.18 | -5.48 | 8.70 |
| $m$-BTe | -22.17 | -9.00 | 15.76 | -4.81 | 10.95 |
| $p$-BTe | -12.55 | -5.68 | 12.47 | -5.42 | 7.05 |

We begin with the pnictaborines and focus on the emergence of aromatic character within this group. The most aromatic was discovered to be 1,3-dihydro-1,3-azaborine, Figure 1(a)-(d). From Table 1, the nuclear independent chemical shifts 1 Å above the molecular plane are NICS$_{ZZ}$(1) $= -26.60$ $ppm$ and NICS$_{ISO}$(1) $= -8.97$ $ppm$, which is consistent with Papadopoulos, et al.[57] These values suggest that 1,3-azaborine is substantially aromatic. Compared with benzene (NICS$_{ZZ}$(1) = -30.44 $ppm$ and NICS$_{ISO}$(1) = -10.14 $ppm$), the prototypical six membered aromatic molecule, 1,3-azaborine is within 3.84 $ppm$ and 1.17 $ppm$ for NICS$_{ZZ}$(1) and NICS$_{ISO}$(1), respectively. The resulting ground state structure is comparable to the previously reported geometrical param-
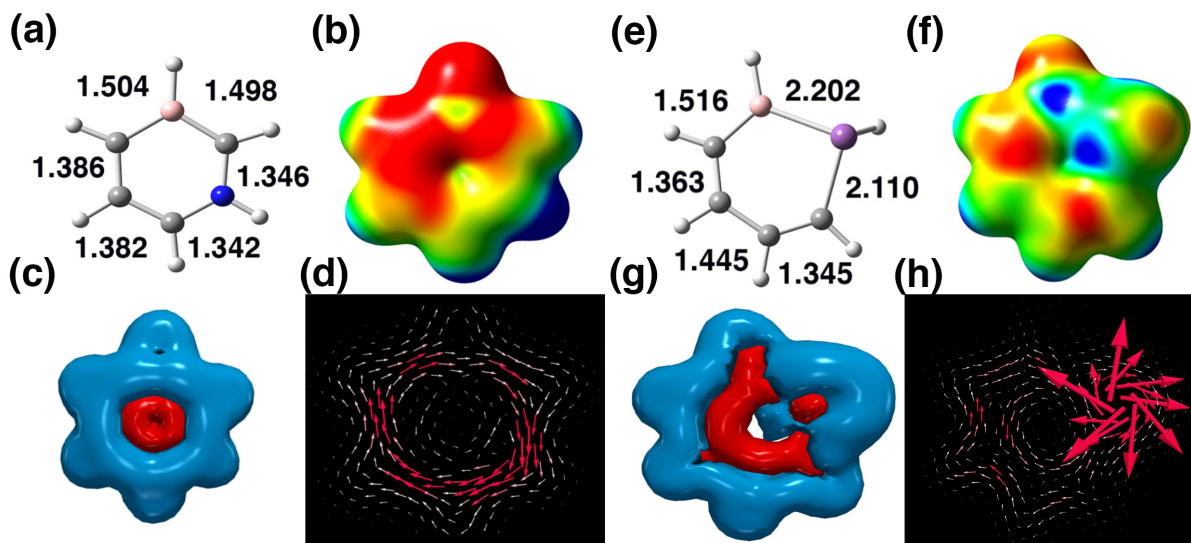
**Fig. 1** Optimized pnictaborines and aromaticity metrics for (a)-(d) 1,3-azaborine (most aromatic) and (e)-(h) 1,2-stibaborine (least aromatic). (a)/(e) optimized ground state geometry and equilibrium bond lengths (Å), (b)/(f) electrostatic potential maps, (c)/(g) signed modulus of the current density displaying the location of diatropic (blue) and paratropic (red) current, and (d)/(h) current maps 1 Å above the molecular plane. The electrostatic potentials are projected onto the ground state electron density to identify regions of charge inhomogeneity. Isosurface values range from $-1.0 \times 10^{-4} - 1.0 \times 10^{-1} a.u.$ (blue to red). The signed modulus of the current is given in $\pm 0.01 \ nAT^{-1}$.

eters in the literature[21,22,57] with bond lengths ranging 1.34-1.50 Å, suggesting $sp^2$ hybridized atoms resembling the seminal synthesis by Liu and coworkers.[6,58] NICS values indicate increased aromaticity for the 1,3-isomer that recedes for 1,2- and 1,4-configurations (Table 1), which is in agreement with GIMIC induced currents.[22,57] The electrostatic potential map of 1,3-azaborine (Fig. 1(b)) displays moderate delocalization around the entire ring. Electron charge density in 1,2-azaborine and 1,4-azaborine isomers tends to localize more strongly, especially in 1,4-azaborine (see SI). Correspondingly, NICS and the average induced current ($\mathscr{J}$) are lower for the ortho- and para-isomers in Table 1. However, the ground state energies are higher for 1,3-azaborine and 1,4-azaborine compared to 1,2-azaborine; energy differences were found to be 88.83 $kJmol^{-1}$ and 122.17 $kJmol^{-1}$, respectively, relative to the ortho-isomer in agreement with Bélanger-Chabot, et al.[59] Because NICS values only describe a single point in space near or around the molecular charge density, it is imperative to corroborate the NICS metric against current maps of the molecule since diatropic or paratropic current is intrinsically a global phenomenon of the molecule itself.[23,28] For 1,3-azaborine, the average induced diatropic current was found to be 15.52 $nAT^{-1}$, while an average paratropic current of -4.80 $nAT^{-1}$ was computed (Table 1). This results in an average total induced current of 10.72 $nAT^{-1}$ for 1,3-azaborine. From the current map of 1,3-azaborine, critical topological features important for sustaining aromaticity in these heterocycles are apparent. Figure 1(d) shows tight toroidal ring current persists over the entire extent of 1,3-azaborine 1 Å above the molecular plane. This is supported by delocalization of the electron density around the hexagonal ring (Figure 1(b)). Furthermore, the signed modulus of the ring current displays large amounts of diatropic current (blue) in Figure 1(c). Notice that the molecular ring current in Figure 1(d) sustains continuous clockwise rotation, which corre-

sponds to the diatropic ring current shown in Figure 1(c). The presence of paratropic current found within the interior of the ring (Figure 1(c), red) offsets the diatropic current, leading to lower overall aromaticity characterized by NICS and the average induced current reported in Table 1.

A sharp decline in aromaticity is apparent when comparing 1,3-azaborine to 1,2-stibaborine, as can be seen in Figure 1(e)-(h) and Table 1. The isotropic chemical shift for 1,2-stibaborine was found to be $NICS_{ISO}(1) = -1.75 \ ppm$ ($NICS_{ZZ}(1) = -2.12 \ ppm$). The most thermodynamically stable antimony boron heterocycle is 1,2-stibaborine, where the ground state energy difference was found to be 114.59 $kJmol^{-1}$ and 14.73 $kJmol^{-1}$ for 1,3-stibaborine and 1,4-stibaborine, respectively. The reduction in aromatic character can be rationalized from a number of factors. The ground state structure displays a trigonal pyramidal geometry at the antimony atom preventing the lone pair from engaging with the $BC_4$ $\pi$-system, Figure 1(e). This engenders charge localization within the ring structure resulting in the formation of two prominent $\pi$-holes (Figure 1(f)). Consequently, the presence of a lone pair at antimony is distinct in the electrostatic potential map (Figure 1(f)) and ring current map (Figure 1(h)) of 1,2-stibaborine. The disruption of molecular ring current arising from pyramidal distortion at antimony (angles of 94.0°, 98.6°, and 102.8°) permits a greater contribution of paratropic ring current, as can be seen in Figure 1(g). As a result, the average diatropic current drops to a value of 10.42 $nAT^{-1}$, while the average paratropic current increases (more negative) to -7.18 $nAT^{-1}$. This yields a lower average total induced current of 3.24 $nAT^{-1}$ for 1,2-stibaborine. Note that 1,4-stibaborine actually has the lowest average diatropic and total current at 9.23 and 2.27 $nAT^{-1}$, respectively (Table 1). From the average current values alone, 1,4-stibaborine features the lowest degree of aromaticity; however, when factoring all metrics collectively (NICS, electrostatic
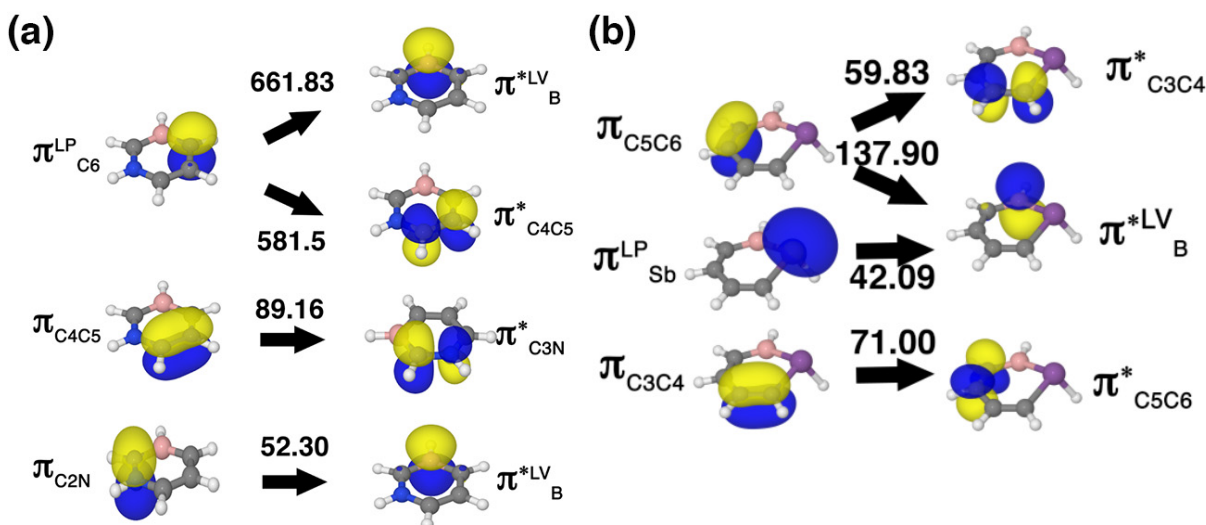
**Fig. 2** Donor-acceptor interactions among Lewis and non-Lewis type NBOs for (a) 1,3-azaborine and (b) 1,2-stibaborine. Each NBO is labeled with an arrow pointing from the Lewis bonding NBOs (principle donor) to antibonding non-Lewis NBOs (principle acceptor). Above the arrows is the stabilization energy resulting from charge delocalization among NBOs in $kJ\ mol^{-1}$.
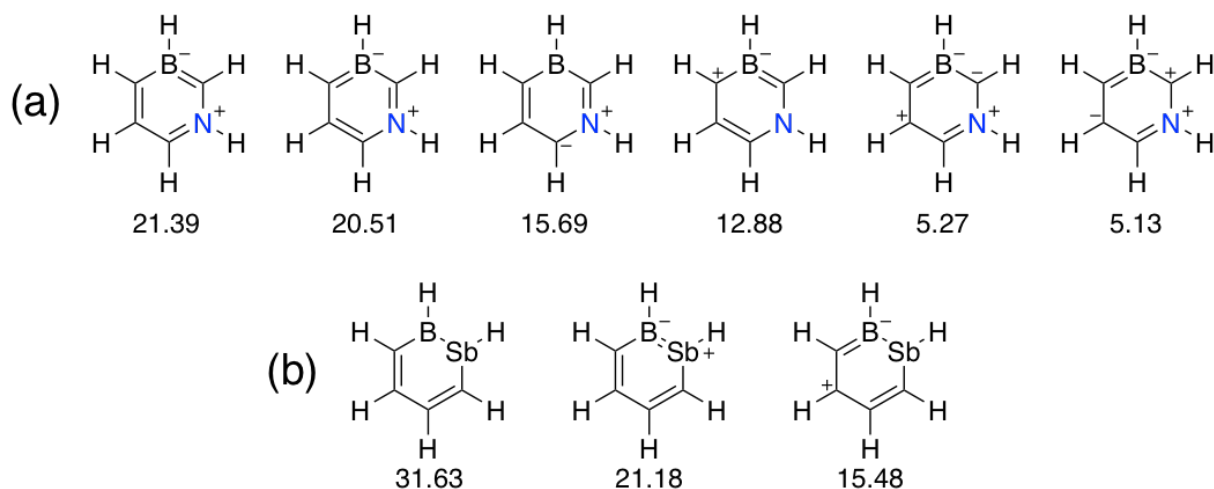


**Fig. 3** Major resonance contributors of (a) 1,3-azaborine and (b) 1,2-stibaborine resulting from NRT analysis. The weighted contribution of each resonance structure is given in (%). Structures contributing less than 5% are not shown.

maps, vector current plots, etc.), the ortho isomer is deemed least aromatic. The distinction is of little importance since the trends for both are very similar and parallel one another. There is an interesting correlation between the formation of the $\pi$-holes in pnictaborines and the modulus of the ring currents. That is, $\pi$-holes coincide with spatial regions where the paratropic current encroaches over diatropic ring current. In fact, this can be seen in the Supplemental Information for all pnictaborines.

The instantiation of ring current can be understood as resulting from $\pi$-$\pi^*$ interactions in an NBO framework, which permits delocalization throughout multiple atoms. NBO analysis partitions the density into "Lewis" and "non-Lewis" orbitals, such that the Lewis NBOs are maximally occupied to provide the best Lewis-like description of the electron density (i.e., optimized specifically to maximize electron population in local bonding arrangements representative of a Lewis structure), while non-Lewis NBOs receive the residual electron density that contributes to delocalization ef-

fects and are the most important contributors to resonance stabilization.[47,48] Interactions between Lewis and non-Lewis NBOs can lead to population shifts, the extent of which is characterized by the stabilization energy magnitude. Large donor-acceptor interactions among Lewis and non-Lewis NBOs indicate significant resonance delocalization corrections and a departure from the idealized Lewis structure picture.[47,48] Note, molecular orbitals (MOs) from linear combinations of atomic orbitals are different from the NBOs discussed here; however, MOs can be expressed in terms of NBOs and often contain contributions from both Lewis and non-Lewis types. NBO analysis is unique, contrasted against valence bond theory or molecular orbital theory, in that no assumption is made regarding the mathematical form of the wavefunction.[60] Moreover, the DFT molecular wavefunctions supply the initial condition for NBO construction, whose solution provides a localized bonding picture between one, two, or more sites characterizing Lewis and non-Lewis type bonding.[48,60]
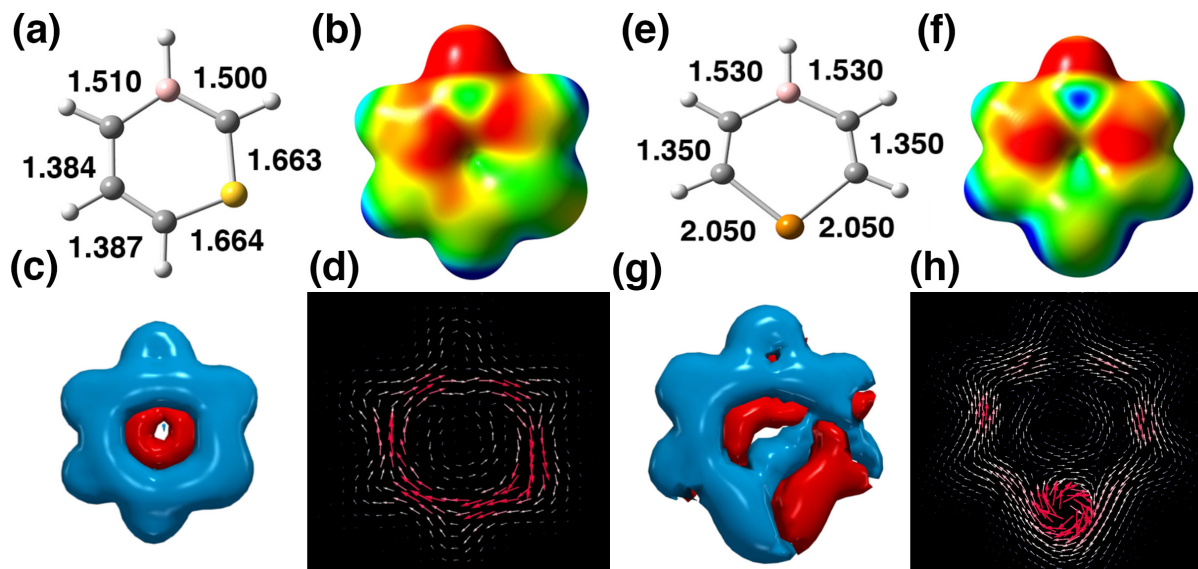
**Fig. 4** Optimized chalcogenaborines and aromaticity metrics for (a)-(d) 1,3-thiaborine (most aromatic) and (e)-(h) 1,4-telluraborine (least aromatic). (a)/(e) optimized ground state geometry and equilibrium bond lengths (Å), (b)/(f) electrostatic potential maps, (c)/(g) signed modulus of the current density displaying the location of diatropic (blue) and paratropic (red) current, and (d)/(h) current maps 1 Å above the molecular plane. The electrostatic potentials are projected onto the ground state electron density to identify regions of charge inhomogeneity. Isosurface values range from $-1.0 \times 10^{-4} - 1.0 \times 10^{-1}$ *a.u.* (blue to red). The signed modulus of the current is given in $\pm 0.01$ $nAT^{-1}$.

Hence, the NBO analysis, presented below, variationally decomposes the orbital moments into chemically recognizable hybrid orbitals that will highlight aromaticity in the unsaturated $BEC_4$ heterocycles.[48,60]

The NBO and NRT analyses of 1,3-azaborine and 1,2-stibaborine are shown in Figures 2 and 3. From NBO analysis of 1,3-azaborine (Fig. 2(a)), the principle delocalization originates from the Lewis $C_6$ lone-pair $\pi_{C_6}^{LP}$-NBO, and the non-Lewis NBOs that accept electrons from $C_6$ are the vacancy on boron ($\pi_{B_{LV}}^*$) and the $C_4 - C_5$ anti-bond ($\pi_{C_4 C_5}^*$). Additional NBOs contribute to the delocalization of electrons for 1,3-azaborine as seen in Figure 2(a). A cyclic pattern of delocalization emerges among donor-acceptor NBOs that is amplified and reciprocated across the heterocycle, which allows for delocalization over the entire ring. However, for the case of 1,2-stibaborine, we observe minimal delocalization into surrounding non-Lewis NBOs, Figure 2(b). The antimony lone pair is involved in donation to the lone-vacancy on boron leading to delocalization on carbon and boron that is asymmetric about the ring. In contrast, planar 1,3-azaborine supports more uniform delocalization suggesting greater resonance overall. In fact, from NRT analysis we can see that the overall resonance for 1,3-azaborine is substantial, especially in contrast to 1,2-stibaborine. Figure 3(a) shows that 1,3-azaborine strongly supports resonance, where the boron and nitrogen elements tend to support unsaturation within the ring. However, 1,2-stibaborine features one resonance contributor with a boron-antimony double bond at 21.18% (Figure 3(b)). NRT analysis shows clearly the lone-pair on antimony interacts little with the $\pi$-system of the molecule with the dominant resonance structure of 31.63%. Consequently, localization on antimony reduces the overall NICS/GIMIC values, features weak clockwise current, and greater paratropicity as seen in the signed modulus of the ring

current (Figure 1, Table 1). In fact, the observations made here (i.e., structure, energetics, NICS, GIMIC, current maps, ring current signed, NBO and NRT analyses) for these two exemplary cases of pnictaborines can be extended to the phosphorus and arsenic congeners as well (see SI for full dataset). The aromaticity of these molecules decreases with increasing atomic number and metallic character of the pnictogen heteroatom. Moreover, the resulting diminution of aromatic character is driven, in large-part, by trigonal pyramidal distortion around the heavier pnictogens. Thus planarity is critical for sustaining aromaticity within pnictaborines while bond regularity seems to be a less important criteria. Energetically the most thermodynamically stable isosteres tend to be ortho-substituted pnictaborines, which is likely driven by complementary boron-pnictogen bonding stabilization. From a global perspective, aromaticity declines within the pnictogen substituted boron heterocycles moving down the group, but this is not observed in the chalcogen substituted analogues.

The chalcogenaborines are distinguished from the pnictaborines by sustaining aromatic character across this group, Table 1. The most aromatic heterocycle 1,3-thiaborine (Figure 4(a)-(d)) has an isotropic nuclear independent chemical shift of $NICS_{ISO}(1) = -8.60$ *ppm*, which is actually fourth by this single metric compared to 1,3-telluraborine ($NICS_{ISO}(1) = -9.00$ *ppm*), 1,3-selenaborine ($NICS_{ISO}(1) = -8.79$ *ppm*), and 1,3-oxaborine ($NICS_{ISO}(1) = -8.66$ *ppm*). However, 1,3-thiaborine has the largest NICS out of plane ($NICS_{ZZ}(1) = -25.36$ *ppm*), and the appearance of the GIMIC current plots (vector and signed modulus) strongly suggest it is the most aromatic. The electrostatic potential of 1,3-thiaborine (Figure 4b) shows moderate delocalization of charge density around the ring and an absence of $\pi$-holes (more generally $\pi$-holes in the chalcogenaborines only show up in the ortho- and para-isomers, see SI). From an ener-
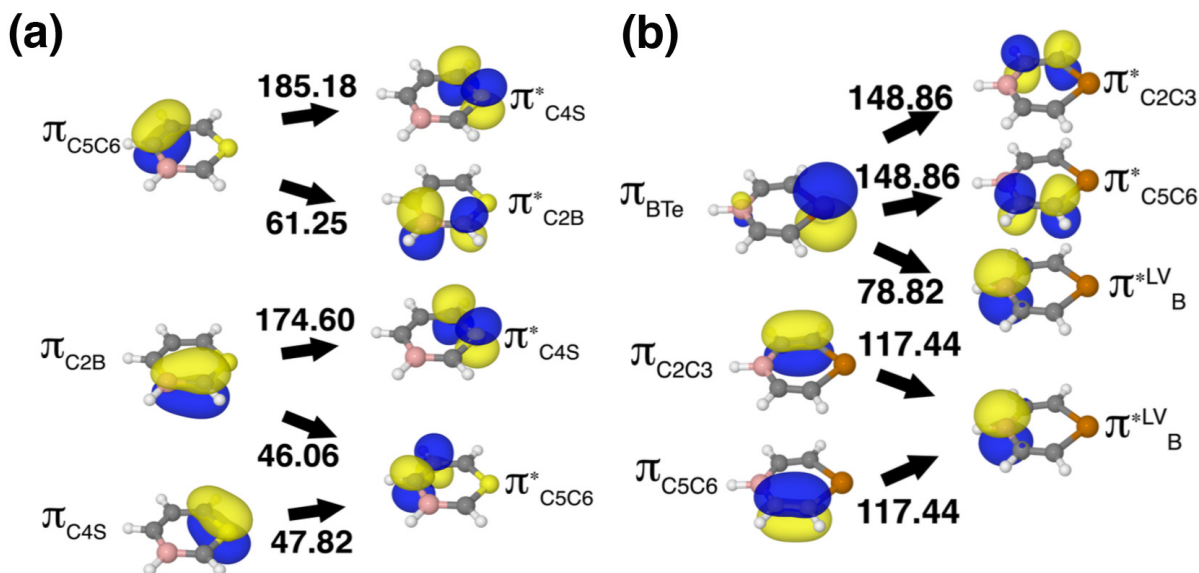
**Fig. 5** Donor-acceptor interactions among Lewis and non-Lewis type NBOs for (a) 1,3-thiaborine and (b) 1,4-telluraborine. Each NBO is labeled with an arrow pointing from the Lewis bonding NBOs (principle donor) to antibonding non-Lewis NBOs (principle acceptor). Above the arrows is the stabilization energy resulting from delocalization among NBOs in $kJ$ $mol^{-1}$.

getic standpoint, the 1,2-isomer is most stable among isosteres of the sulfur boron heterocycles, with ground state energy differences of 105.89 $kJmol^{-1}$ and 78.63 $kJmol^{-1}$ for 1,3-thiaborine and 1,4-thiaborine, respectively. This trend is generally observed for all chalcogenaborines, with the exception of the oxygen-boron heteroarenes that have a reversed energetic ordering with 1,4-oxaborine being most stable (energy differences of 94.44 $kJmol^{-1}$ for 1,2-oxaborine and 66.75 $kJmol^{-1}$ for 1,3-oxaborine). From the current map of 1,3-thiaborine (Figure 4(d)), we see strong toroidal circulation of current density in the clockwise direction suggesting pronounced diatropic current. This is corroborated with the modulus of the ring current shown in Figure 4(c). It is clear the diatropic ring current dominates the paratropic current within 1,3-thiaborine. The average diatropic and paratropic currents were determined to be 15.90 $nAT^{-1}$ and -4.90 $nAT^{-1}$, respectively, yielding an average total induced current of 11.00 $nAT^{-1}$ for 1,3-thiaborine (Table 1). This is very close to benzene ($\mathscr{J}^{Dia}$ = 17.09 $nAT^{-1}$, $\mathscr{J}^{Para}$ = −4.98 $nAT^{-1}$, $\mathscr{J}^{Total}$ = 12.06 $nAT^{-1}$) indicating 1,3-thiaborine is very aromatic. Furthermore, the absence of $\pi$-holes in 1,3-thiaborine, which are accompanied with paratropic current, permits sustainment of strong aromaticity within this molecule. Note that 1,3-selenaborine has comparable aromaticity values and is also considered very aromatic. The primary differentiators are the spatial plots of ring current (signed modulus and vector plots), which indicate thiaborine is more aromatic (see SI).

Aromaticity becomes reduced significantly in 1,4-telluraborine, Figure 4(e)-(h). The appearance of a $\pi$-hole forms over the electron-deficient boron atom within the ring, and the electrostatic potential map shows strong localization around the carbon-carbon bond (Fig. 4(f)). These two effects lower the overall aromaticity within this molecule, with $NICS_{ISO}(1) = -5.68$ $ppm$ and $NICS_{ZZ}(1) = -12.55$ $ppm$. Surprisingly, the NICS values sug-

gest moderate aromatic character for 1,4-telluraborine (especially compared to the less aromatic pnictaborines), yet the current map shows disjointed, weak diatropic current. The lone pair forms a strong vortex over the tellurium atom while the diatropic current vanishes over boron corroborating the electrostatic potential map (Figure 4(f)-(h)). Also, the ring current modulus displays significant paratropic current intertwined with diatropic current, leading to an average total induced current of 7.05 $nAT^{-1}$. This value is nearly half the total induced current of benzene suggesting that 1,4-telluraborine is weakly aromatic. Further insight can be gleaned from a streamline plot of the current in 1,4-telluraborine, which displays additional underlying vortices in the molecule extending outward 1 Å (SI Fig. 10). Collectively, the current data suggests that the overall aromatic character of 1,4-telluraborine is notably weaker than predicted by NICS alone, Table 1. NICS values can hint of aromaticity, but a molecular property cannot be reduced to a single point in general, which emphasizes a shortcoming in their use exclusively for the characterization of aromaticity. [23,28]

The aromatic character in chalcogenaborines is further highlighted by the NBO and NRT analyses for these two exemplary cases. Figures 5 and 6 show the results for 1,3-thiaborine and 1,4-telluraborine, respectively. In 1,3-thiaborine, we can see the primary Lewis donor-acceptors contributing to the substantial aromaticity in this molecule (Figure 5(a)). The principle delocalization originates from donors $\pi_{C_5C_6}$ and $\pi_{C_2B}$ to the same acceptor $\pi^*_{C_4S}$. In both cases, two NBOs from vicinal positions on the hexagonal ring delocalize to NBOs on the other side. Delocalization of $\pi$-electrons from across the ring admixing with an adjoining acceptor NBO ensures resonance within this molecule. Weaker mixing of donors $\pi_{C_5C_6}$ and $\pi_{C_4S}$ to acceptors $\pi^*_{C_2B}$ and $\pi^*_{C_5C_6}$ results in a cyclic delocalization pattern that reciprocates delocalization around the hexagonal ring, Figure 5(a). Consequently, the
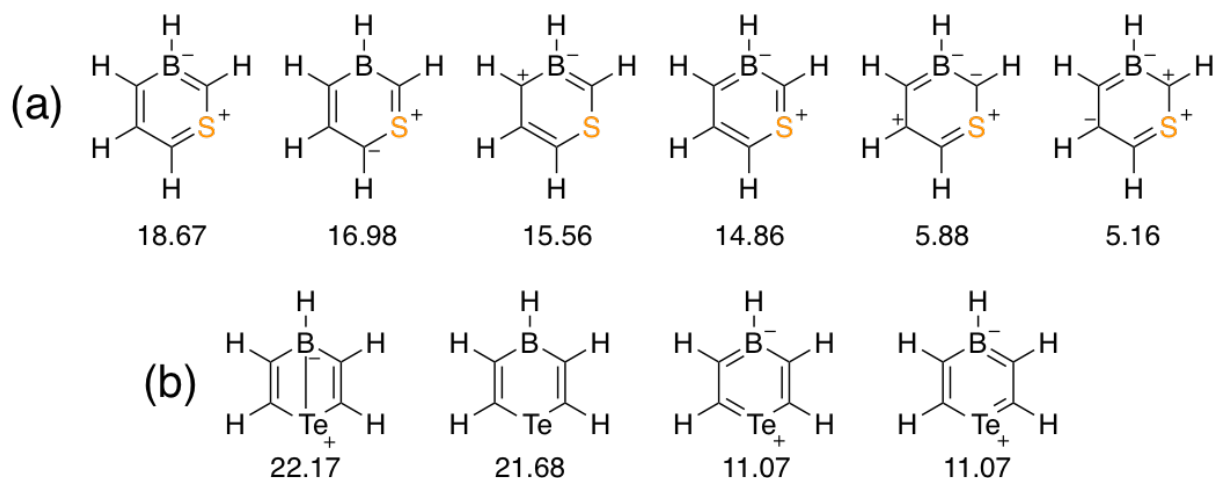
**Fig. 6** Major resonance contributors of (a) 1,3-thiaborine and (b) 1,4-telluraborine resulting from NRT analysis. The weighted contribution of each resonance structure is given in (%). Structures contributing less than 5% are not shown.

cyclic delocalization pattern observed in 1,3-thiaborine enables substantial resonance to form as displayed by the NRT analysis in Figure 6(a). Note, only a single resonance structure features two lone pairs on sulfur contributing 15.56%. Similar cyclic delocalization patterns are observed in the NBO and NRT analyses of other chalcogenaborines (see SI). However, 1,4-telluraborine shows an unusual pattern from the other isomers and congeners. First, the principle delocalization originates from a unique donor $\pi_{BTe}$ para-NBO that delocalizes into vicinal $\pi^*_{C_2C_3}$ and $\pi^*_{C_5C_6}$ acceptor NBOs with stabilization energy of 148.86 $kJmol^{-1}$, Figure 5(b). Interestingly, there is a weaker delocalization from donor $\pi_{BTe}$ to acceptor $\pi^{*LV}_B$ NBO of 78.82 $kJmol^{-1}$. The $\pi$-NBOs of each carbon bond delocalize into the electropositive $\pi^{*LV}_B$-NBO. Overall, these effects decrease the overall aromaticity within 1,4-telluraborine. NRT analysis shows that the lead resonance structure at 22.17% features a long Dewar-like bond forming between both heteroatoms, Figure 6(b). This interaction between boron and tellurium is misleading as it pertains to the para-NBO discussed above, and results from intramolecular charge transfer between the two heteroatoms rather than an actual bond. Moreover, 1,4-telluraborine features a competing resonance structure that supports lone-pair and lone-valence on boron and tellurium at 21.68%. Overall 1,4-telluraborine is perhaps best described as an intramolecular frustrated Lewis-pair reminiscent of borylated vinyl telluroethers.[61] While 1,4-telluraborine features the lowest aromatic character among the chalcogen substituted boron heterocycles, this molecule supports conjugation as seen in the lower contributing resonance structures (Figure 6(b)). In fact, generally all of the chalcogenaborines tend to support strong aromatic character enabled by lone-pairs from chalcogen elements.

## 4 Conclusions

The aromatic character of pnictogen and chalcogen substituted boron heterocycles was investigated with ab-initio DFT employing a bevy of approaches including GIAO-NICS, GIMIC, NBO and NRT analyses. We observe a general decline of aromatic character within the pnictaborines descending down the group. The

reduction of aromaticity is accompanied with pyramidalization at the heavier pnictogen elements such as arsenic and antimony. Consequently, the overall NICS/GIMIC values decline and electrostatic potential maps display $\pi$-holes within the heterocycle. Current maps and moduli of the ring current show variations in diatropic and paratropic current resulting from charge localization and delocalization, dependent upon where electropositive boron or the electronegative pnictogen is placed within the heterocycle. Resonance within pnictaborines depends on $\pi$-$\pi^*$ NBO interactions that sustain a cyclic delocalization pattern, especially in the more aromatic 1,3-configurations. Thus, trigonal pyramidal distortions, paratropic $\pi$-holes, and weaker diatropic current within pnictaborines increase with the larger congeners. In contrast, chalcogenaborines display general aromatic character across all heterocycles with only a weak reduction in aromaticity for heavier chalcogen elements. The most aromatic molecule among all heterocycles discussed within this article is 1,3-thiaborine. It shows a lack of $\pi$-holes resulting from greater charge delocalization, sustained diatropic current across the exterior of the molecule, a reduction of paratropic current, high NICS values, and a planar structure. These general qualities are present in many of the chalcogenaborines, leading to a more consistent aromaticity of the group as a whole. This comprehensive study of hybrid benzene analogues is the first of its kind and provides a unique perspective on the aromaticity of many unknown molecules to guide the experimental efforts of synthetic chemists.

## Conflicts of interest

There are no conflicts to declare.

## Acknowledgements

# Notes and references

1  M. J. S. Dewar and R. Dietz, *Tetrahedron Lett.*, 1959, 21–23.

2  M. J. S. Dewar and R. Dietz, *J. Chem. Soc.*, 1960, 1344–1347.

3  M. J. S. Dewar and P. A. Marr, *J. Am. Chem. Soc.*, 1962, **84**, 3782–3782.

4  D. G. White, *J. Am. Chem. Soc.*, 1963, **85**, 3634–3636.

5  K. M. Davies, M. J. S. Dewar and P. Rona, *J. Am. Chem. Soc.*, 1967, **89**, 6294–6297.

6  S. Xu, L. N. Zakharov and S.-Y. Liu, *J. Am. Chem. Soc.*, 2011, **133**, 20152–20155.

7  T. Zeng, N. Ananth and R. Hoffmann, *J. Am. Chem. Soc.*, 2014, **136**, 12638–12647.

8  D. W. Stephan, *J. Am. Chem. Soc.*, 2015, **137**, 10018–10032.

9  P. Zhao, D. O. Nettleton, R. G. Karki, F. J. Zécri and S.-Y. Liu, *ChemMedChem*, 2017, **12**, 358–361.

10  J. Chen, Z. Bajko, J. W. Kampf and A. J. Ashe, *Organometallics*, 2007, **26**, 1563–1564.

11  H. Saito, S. Otsuka, K. Nogi and H. Yorimitsu, *J. Am. Chem. Soc.*, 2016, **138**, 15315–15318.

12  B. Su and R. Kinjo, *Synthesis*, 2017, **49**, 2985–3034.

13  S. Yruegas, D. C. Patterson and C. D. Martin, *Chem. Commun.*, 2016, **52**, 6658–6661.

14  S. Yruegas and C. D. Martin, *Chem. Eur. J*, 2016, **22**, 18358–18361.

15  J. H. Barnard, P. A. Brown, K. L. Shuford and C. D. Martin, *Angew. Chem. Int. Ed.*, 2015, **54**, 12083–12086.

16  Z. Chen, C. S. Wannere, C. Corminboeuf, R. Puchta and P. v. R. Schleyer, *Chem. Rev.*, 2005, **105**, 3842–3888.

17  V. L. Murphy, A. Reyes and B. Kahr, *J. Am. Chem. Soc.*, 2016, **138**, 25–27.

18  E. R. Abbey, L. N. Zakharov and S.-Y. Liu, *J. Am. Chem. Soc.*, 2008, **130**, 7250–7252.

19  I. V. Omelchenko, O. V. Shishkin, L. Gorb, J. Leszczynski, S. Fias and P. Bultinck, *Phys. Chem. Chem. Phys.*, 2011, **13**, 20536–20548.

20  A. Chrostowska, S. Xu, A. N. Lamm, A. Maziére, C. D. Weber, A. Dargelos, P. Baylére, A. Graciaa and S.-Y. Liu, *J. Am. Chem. Soc.*, 2012, **134**, 10279–10285.

21  M. Baranac-Stojanović, *Chem. Eur. J.*, 2014, **20**, 16558–16565.

22  M. Stojanoviá and M. Baranac-Stojanoviá, *J. Org. Chem.*, 2016, **81**, 197–205.

23  P. Lazzeretti, *Phys. Chem. Chem. Phys.*, 2004, **6**, 217–223.

24  F. London, *J. Phys. Radium*, 1937, **8**, 397–409.

25  V. Elser and R. Haddon, *Nature*, 1987, **325**, 792–794.

26  J. R. Cheeseman, G. W. Trucks, T. A. Keith and M. J. Frisch, *J. Chem. Phys.*, 1996, **104**, 5497–5509.

27  P. v. R. Schleyer, C. Maerker, A. Dransfeld, H. Jiao and N. J. R. van Eikema Hommes, *J. Am. Chem. Soc.*, 1996, **118**, 6317–6318.

28  S. Van Damme, G. Acke, R. W. A. Havenith and P. Bultinck, *Phys. Chem. Chem. Phys.*, 2016, **18**, 11746–11755.

29  G. Acke, S. Van Damme, R. W. A. Havenith and P. Bultinck, *J.*

30  M. P. Johansson, J. Jusélius and D. Sundholm, *Angew. Chem. Int. Ed.*, 2005, **44**, 1843–1846.

31  S. Taubert, D. Sundholm, J. Jusélius, W. Klopper and H. Fliegl, *J. Phys. Chem. A*, 2008, **112**, 13584–13592.

32  H. Fliegl, D. Sundholm, S. Taubert, J. Jusélius and W. Klopper, *J. Phys. Chem. A*, 2009, **113**, 8668–8676.

33  H. Fliegl, S. Taubert, O. Lehtonen and D. Sundholm, *Phys. Chem. Chem. Phys.*, 2011, **13**, 20500–20518.

34  H. Fliegl, F. Pichierri and D. Sundholm, *J. Phys. Chem. A*, 2015, **119**, 2344–2350.

35  H. Fliegl, J. Jusélius and D. Sundholm, *J. Phys. Chem. A*, 2016, **120**, 5658–5664.

36  W. Kohn and L. J. Sham, *Phys. Rev.*, 1965, **140**, A1133–A1138.

37  P. Hohenberg and W. Kohn, *Phys. Rev.*, 1964, **136**, B864–B871.

38  M. J. Frisch, G. W. Trucks, H. B. Schlegel, G. E. Scuseria, M. A. Robb, J. R. Cheeseman, G. Scalmani, V. Barone, G. A. Petersson, H. Nakatsuji, X. L. M. Caricato, A. Marenich, J. Bloino, B. G. Janesko, R. Gomperts, B. Mennucci, H. P. Hratchian, J. V. Ortiz, A. F. Izmaylov, J. L. Sonnenberg, D. Williams-Young, F. Ding, F. Lipparini, F. Egidi, J. Goings, B. Peng, A. Petrone, T. Henderson, D. Ranasinghe, V. G. Zakrzewski, J. Gao, N. Rega, G. Zheng, W. Liang, M. Hada, M. Ehara, K. Toyota, R. Fukuda, J. Hasegawa, M. Ishida, T. Nakajima, Y. Honda, O. Kitao, H. Nakai, T. Vreven, K. Throssell, J. J. A. Montgomery, J. E. Peralta, F. Ogliaro, M. Bearpark, J. J. Heyd, E. Brothers, K. N. Kudin, V. N. Staroverov, T. Keith, R. Kobayashi, J. Normand, K. Raghavachari, A. Rendell, J. C. Burant, S. S. Iyengar, J. Tomasi, M. Cossi, J. M. Millam, M. Klene, C. Adamo, R. Cammi, J. W. Ochterski, R. L. Martin, K. Morokuma, O. Farkas, J. B. Foresman and D. J. Fox, Gaussian Inc. Wallingford CT 2016.

39  J. Heyd and G. E. Scuseria, *J. Chem. Phys.*, 2004, **120**, 7274–7280.

40  J. Heyd and G. E. Scuseria, *J. Chem. Phys.*, 2004, **121**, 1187–1192.

41  J. Heyd, J. E. Peralta, G. E. Scuseria and R. L. Martin, *J. Chem. Phys.*, 2005, **123**, 174101.

42  J. Heyd, G. E. Scuseria and M. Ernzerhof, *J. Chem. Phys.*, 2006, **124**, 219906.

43  L. A. Curtiss, M. P. McGrath, J. Blaudeau, N. E. Davis, R. C. B. Jr. and L. Radom, *J. Chem. Phys.*, 1995, **103**, 6104–6113.

44  W. R. Wadt and P. J. Hay, *J. Chem. Phys.*, 1985, **82**, 284–298.

45  D. Rappoport and F. Furche, *J. Chem. Phys.*, 2010, **133**, 134105.

46  F. Neese, *Wiley Interdisciplinary Reviews: Computational Molecular Science*, 2012, **2**, 73–78.

47  E. D. Glendening, J. K. Badenhoop, A. E. Reed, J. E. Carpenter, A. Bohmann, C. M. Morales, C. R. Landis and F. Weinhold, *NBO 6.0*, Theoretical Chemistry Institute, University of Wisconsin, Madison, 2013.

48  E. D. Glendening, C. R. Landis and F. Weinhold, *J. Comput.*

*Comput. Chem.*, 2018, **39**, 511–519.

*Chem.*, 2013, **34**, 1429–1437.

49 E. D. Glendening and F. Weinhold, *J. Comput. Chem.*, 1998, **19**, 593–609.

50 E. D. Glendening and F. Weinhold, *J. Comput. Chem.*, 1998, **19**, 610–627.

51 E. D. Glendening, J. K. Badenhoop and F. Weinhold, *J. Comput. Chem.*, 1998, **19**, 628–646.

52 C. Adamo and V. Barone, *J. Chem. Phys.*, 1999, **110**, 6158–6170.

53 M. Ernzerhof and G. E. Scuseria, *J. Chem. Phys.*, 1999, **110**, 5029–5036.

54 K. A. Peterson, D. Figgen, E. Goll, H. Stoll and M. Dolg, *J.*

*Chem. Phys.*, 2003, **119**, 11113–11123.

55 F. Weigend and R. Ahlrichs, *Phys. Chem. Chem. Phys.*, 2005, **7**, 3297–3305.

56 F. Weigend, *Phys. Chem. Chem. Phys.*, 2006, **8**, 1057–1065.

57 A. G. Papadopoulos, N. D. Charistos, K. Kyriakidou and M. P. Sigalas, *J. Phys. Chem. A*, 2015, **119**, 10091–10100.

58 S. Xu, Y. Zhang, B. Li and S.-Y. Liu, *J. Am. Chem. Soc.*, 2016, **138**, 14566–14569.

59 G. Bélanger-Chabot, H. Braunschweig and D. K. Roy, *Eur. J. Inorg. Chem.*, 2017, 4353–4368.

60 F. Weinhold, *J Comput. Chem.*, 2012, **33**, 2363–2379.

61 F. A. Tsao and D. W. Stephan, *Dalton Trans.*, 2015, **44**, 71–74.